

# Transformation-Dependent Adversarial Attacks

Yaoteng Tan, Zikui Cai, and M. Salman Asif

University of California Riverside

{ytan073, zcai032, sasif}@ucr.edu

## Abstract

*We introduce transformation-dependent adversarial attacks, a new class of threats where a single additive perturbation can trigger diverse, controllable mis-predictions by systematically transforming the input (e.g. scaling, blurring, compression). Unlike traditional attacks with static effects, our perturbations embed metamorphic properties to enable different adversarial attacks as a function of the transformation parameters. We demonstrate the transformation-dependent vulnerability across models (e.g. convolutional networks and vision transformers) and vision tasks (e.g. image classification and object detection). Our proposed geometric and photometric transformations enable a range of targeted errors from one crafted input (e.g. higher than 90% attack success rate for classifiers). We analyze effects of model architecture and type/variety of transformations on attack effectiveness. This work forces a paradigm shift by redefining adversarial inputs as dynamic, controllable threats. We highlight the need for robust defenses against such multifaceted, chameleon-like perturbations that current techniques are ill-prepared for.*

## 1. Introduction

Adversarial attacks on deep neural networks have traditionally been studied through the lens of imperceptible perturbations that can fool models into misclassifying inputs [11, 12, 16, 22, 27, 30, 48, 49, 53, 55]. In many real cases, inputs can undergo different transformations due to changes in viewpoint, lighting conditions, and resolution with little to no perceptual change. Prior work has attempted to make adversarial attacks robust to such input transformations by optimizing over the expectation of the attack objective under a distribution of transformations. For instance, the expectation over transformation (EOT) framework [1] seeks transformation-invariant attacks that remain effective regardless of how the input is transformed.

In this work, we explore an entirely different dimension of transformation-dependent adversarial attacks. Rather than striving for invariance, we unveil a formidable new

threat where a single, carefully crafted perturbation can induce a wide variety of targeted misclassifications by transforming the input image. Imagine a seemingly benign image that turns into an adversarial example with different target labels when resized, rotated, or recolored with different parameters. This redefines what it means for an input to be adversarial - the adversarial nature is not simply an intrinsic property, but a complex capability imbued by the perturbation to react differently under different transformations. Figure 1 presents some examples of transformation-dependent adversarial attacks, where a single perturbation can provide different labels as a function of the transformation on the perturbed image.

Such controlled, multifaceted adversarial attacks pose a profound threat that current defenses are woefully unprepared for. Our results demonstrate the significant vulnerability of modern deep learning models to this new class of attacks. We show that a single additive perturbation can seamlessly embed a remarkable diversity of targeted attacks triggered by predefined transformations of the input. The implications are severe - adversarial attacks now escape the realm of isolated, static perturbations and become dynamic, controllable threats that can manifest in drastically different ways depending on how the input is transformed.

We summarize our main contributions as follows.

- We introduce the novel concept of transformation-dependent adversarial attacks, where a single additive perturbation can embed multiple targeted attacks that are triggered by predefined transformations on the input image (e.g. scaling, blurring, gamma correction).
- We demonstrate the versatility of such attacks using extensive experiments with different models and input transformations that provide diverse, controllable attack effects from a single perturbation.
- Our experiments highlight different factors that influence the effectiveness of such controllable perturbations, e.g., the choice of transform function, model architecture, and the number of targeted attacks that can be embedded.
- We demonstrate that the proposed transformation-dependent attacks can bypass some existing defenses

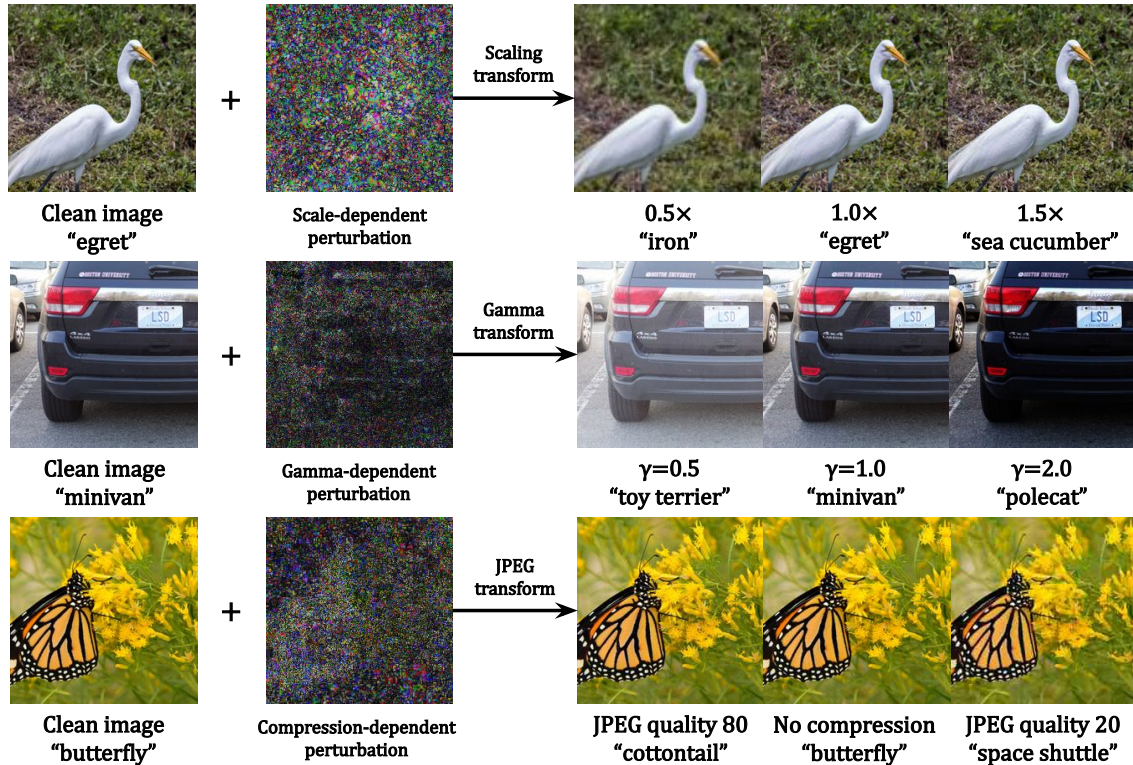


Figure 1. Examples of transformation-dependent adversarial attacks. A single adversarial perturbation added to clean image can offer multiple attack effects for different (desired) image transformations. *First row*: Targeted attacks are triggered by scaling at  $0.5\times$  and  $2\times$ , with clean label at  $1\times$ . Scaled images in the first row will have different sizes after scaling, but we present their resized versions for better display. *Second row*: Attacks triggered with  $\gamma = 0.5, 2$  in gamma correction, while providing the clean label with  $\gamma = 1$ . *Third row*: Attacks triggered with JPEG image compression quality factor 80, 20, while providing the clean label with no compression. The perturbation in all examples is bounded by  $\ell_\infty \leq 10$ ; the magnitude is amplified  $30\times$  for better visualization.

(e.g., adversarial training, randomized smoothing) and succeed with effective black-box transfer.

- We showcase the real-world implications by extending transformation-dependent attacks to the object detection task, achieving selective hiding of objects based on the applied transformation.

Our attack formulation represents the initial endeavor to integrate multiple attack effects into one single adversarial perturbation, which can be dynamically activated in coordination with image transformations, enabling adversarial attack in a controllable manner. Our work questions the fundamental assumption in adversarial machine learning — that an input is either benign or adversarial. Our work forces a conceptual paradigm shift, as adversarial perturbations can now encode metamorphic properties that reveal different attack effects based on transformations applied to the input. Defenses can no longer simply aim to detect static perturbations, but must grapple with the chameleon-like nature of our transformation-dependent adversarial attacks.

## 2. Related Work

### 2.1. Known properties of adversarial examples

Adversarial examples possess several intriguing properties that have been extensively studied in the literature. Besides imperceptibility, researchers have explored and imposed several other properties, such as transferability, universality, and transformation robustness. An intriguing property of adversarial examples is their transferability across different models [34, 47]. Adversarial examples generated for one model can often fool other models trained on the same task, even if they have different architectures or were trained on different datasets. To enhance transferability, ensemble-based and momentum-based attacks are proposed. Researchers have also discovered the existence of universal adversarial perturbations (UAPs) [32], which are single noise patterns that can cause mis-classification across a wide range of input samples, rather than being tailored to individual samples. While UAPs underscore the potential for broad applicability of a single perturbation, they do

not inherently address dynamic control over the prediction outcomes based on input transformations. A foundational area of relevance is the body of work centered on the robustness of machine learning models against input transformations. Expectation Over Transformation (EOT) provides a framework for generating adversarial examples that remain effective under a range of transformations, such as rotation and scaling[1]. This methodology enables physical attacks by considering the variability of real-world inputs in crafting adversarial attacks. These studies collectively highlight the evolving understanding of adversarial perturbations, however they are focusing on singular attacks and do not provide insights on dynamically controllable perturbations which we specifically investigate in this paper.

## 2.2. Differentiable image transformations

The core premise of transformation-dependent attacks relies on applying differentiable transformations to input images during the adversarial optimization process. A wide range of image transformations have been adapted to differentiable forms, enabling their seamless integration into gradient-based optimization frameworks. Geometric transformations like scaling, translation, and rotation are differentiable thanks to the availability of interpolation techniques like bilinear and bicubic interpolation, which can be expressed as differentiable operations [21]. Photometric transformations such as gamma correction, brightness/contrast adjustments, and color space augmentations can be made differentiable by formulating them as point-wise operations on the input tensor. Gaussian blurring, which is non-differentiable due to the discrete nature of the kernel, can be approximated using isotropic kernels expressed as a linear combination of Gaussian basis functions, enabling differentiation. Even low-level operations like JPEG compression, which involves quantization, can be approximated using differentiable formulations that model the quantization effects [42]. The choice of transformations is motivated by their prevalence in real-world imaging conditions and data augmentation pipelines. By composing a diverse set of spatial, photometric, and signal transformations, we can optimize for adversarial perturbations that exhibit controllable behavior under a wide range of input corruptions that may occur during deployment.

## 2.3. Image transformation in adversarial attacks

In adversarial attack literature, image transformations have primarily been leveraged for two purposes: 1) Generating transformation-invariant adversarial examples that remain effective under input corruptions [1, 23, 24], and transferable adversarial examples that remain adversarial across different models [12, 27, 48, 49, 53, 55]. This line of works seeking robust adversarial examples that provide consistent attack effects under various conditions. 2) Generat-

ing adversarial examples via simple geometric transformations [5, 15, 36, 51]. Beyond  $\ell_\infty$ -norm bounded perturbation, this line of works seeking adversarial examples in the neighbour of transformed images by optimizing transformation parameter. While they provide observations of deep neural network can be fooled by simple geometric transformation of colorization, the attacks are limited to certain transformation parameters and some requires to change the image semantic content [51] or deviated from natural image color distribution [5], which ignore the discussion on practical scenarios. In contrast, our work exploits the more general and diverse image transformations, covering spatial, photometric, and compression transformations to craft adversarial perturbations capable of dynamically altering their effects based on the transformation applied. Introducing controllable attack effects by transforming the input in various ways.

## 3. Method

### 3.1. Preliminaries

We consider additive perturbation form of adversarial attacks [16, 30, 44] that generate adversarial example as  $\mathbf{x} + \delta$ , where  $\delta$  is an adversarial perturbation for a given image  $\mathbf{x}$ . In the benign case, a well-trained model  $f$  that provides correct prediction  $f(\mathbf{x}) = y$ , can provide incorrect prediction that does not match the correct label  $f(\mathbf{x} + \delta) \neq y$  in the context of untargeted adversarial attacks; or provide the desired target label  $f(\mathbf{x}^*) = y^*$  in targeted attacks. To keep the perturbation imperceptible,  $\delta$  is usually bounded within the  $\ell_p$  norm ball  $\|\delta\|_p \leq \varepsilon$ . In general, targeted adversarial attacks can be generated as a solution of the following optimization problem:

$$\min_{\delta} \mathcal{L}(f(\mathbf{x} + \delta), y^*) \quad \text{s.t.} \quad \|\delta\|_p \leq \varepsilon. \quad (1)$$

A general choice for loss function  $\mathcal{L}$  is the training loss for the corresponding tasks. Several algorithms have been proposed to solve this optimization problem, notable examples include FGSM [16], PGD [30], MIM [11] and Auto-Attack [8, 9]. In this work, we focus on PGD attacks for their simplicity and effectiveness. PGD iteratively solves the attack optimization problem as

$$\delta^{t+1} = \Pi_{\varepsilon} (\delta^t - \alpha \text{sign}(\nabla_{\delta} \mathcal{L}(f(\mathbf{x} + \delta^t), y^*))), \quad (2)$$

where  $\delta^t$  denotes perturbation at iteration  $t$  that is updated using sign of gradient with step size  $\alpha$ .  $\Pi_{\varepsilon}$  denotes an operator that projects the updated  $\delta^t$  back to the  $\ell_p$ -norm ball and obtain  $\delta^{t+1}$ .

### 3.2. Transformation-dependent attacks

Let us define the image transform function as  $T(\mathbf{x}; \theta)$  that transform the input image  $\mathbf{x}$  according to the given transform parameter  $\theta$ . Applying the transform function over



clean input images does not cause significant degradation in the accuracy of networks that are properly trained with data augmentation techniques [21, 31, 39]. In other words, the output of the transformed images remains same as the original image:

$$f(T(\mathbf{x}; \theta)) \sim y. \quad (3)$$

To introduce image transformation-dependent effects in adversarial examples, we incorporate the transformation function in the attack generation. Specifically, we aim for transformation-dependent targeted attacks with target label  $y_i^*$  for the corresponding transformation parameter  $\theta_i$ .

In the most general form,  $\theta$  and  $y^*$  represent two vectors with  $N$  targets embedded in the transformation-dependent attacks as  $\theta = \{\theta_i\}_{i=1}^N$ ,  $y^* = \{y_i^*\}_{i=1}^N$ . The attacker can provide a mapping **parameter-target** pairs that trigger the label  $y_i^*$  for the transformation parameter  $\theta_i$ . The transformation parameter can be assigned a fixed single value or the value can be drawn from a range of target values at random. We can generate a single transformation-dependent perturbation  $\delta$  as a solution of the following optimization problem:

$$\min_{\delta} \sum_i \mathcal{L}(f(T(\mathbf{x} + \delta; \theta_i)), y_i^*) \quad \text{s.t. } \|\delta\|_p \leq \varepsilon. \quad (4)$$

At the test time, the perturbed image can be created as  $\mathbf{x}^* = \mathbf{x} + \delta$  and the transformation-dependent adversarial examples can be created as  $T(\mathbf{x}^*; \theta_i)$  and attacks can be triggered by providing malicious  $\theta_i$ , resulting in transformation-dependent effects.

### 3.3. Transform functions

The first desired property for generating adversarial attacks is the differentiability of the selected transforms  $T(\mathbf{x}; \theta)$  so that it can be used with gradient-based attack algorithms and the gradient of loss function with respect to  $\delta$  can be written as  $\nabla_{\delta} \mathcal{L}(f(T(\mathbf{x} + \delta; \theta)), y^*) = \frac{\partial \mathcal{L}}{\partial f} \frac{\partial f}{\partial T} \frac{\partial T}{\partial \delta}$ . The second key property is controllability, transformation is controlled by  $\theta$ . The attacker can customize transformation-dependent effects according to  $\theta$  provided to transform function.

Based on these two properties, we adopt a wide range of image transformation techniques as transform functions, covering spatial, photometric transformations, and image compression. Here we focus our discussion on scaling, blurring, gamma, and JPEG compression that we mainly used in the experiment. In scaling, transformation parameter is scaling factor  $S$ ,  $T$  transform image  $\mathbf{x} \in \mathbb{R}^{H \times W \times 3}$  into  $T(\mathbf{x}; \theta = S) \in \mathbb{R}^{SH \times SW \times 3}$ . Commonly used scaling methods like bilinear and bicubic interpolations are differentiable operations. In blurring, typically Gaussian blur, the transformation parameter is the standard deviation  $\sigma$  used to create the Gaussian kernel and the transformed image can be represented as  $T(\mathbf{x}; \theta = \sigma)$ . Gamma correction,  $T(\mathbf{x}; \theta = \gamma) = A\mathbf{x}^{\gamma}$  is also a differentiable operation.

## 4. Experiments

In this section, we present main results of transformation-dependent adversarial attacks. We demonstrate that our attack formulation is effective with a wide range of transformations across models built in different designs. We also provide studies for properties of such attacks, including target-specific loss landscape, capacity for embedding transformation-dependent attacks of one perturbation and effectiveness against robustified models and blackbox models. Beyond the success on image classification task, we further show generalizability of our attack formulation over the more complex object detection task.

### 4.1. Experiment setup

**Models and dataset.** We utilize pretrained image classification models from Pytorch Torchvision [35], which provides models pretrained on ImageNet dataset [10] for a variety of families and architectures. Models are trained with data augmentation techniques including random cropping, rotation, flipping and color jittering. We select models from different families that cover Convolutional Neural Networks (CNNs) and Vision Transformer (ViT): {VGG-19-BN [43], ResNet-50 [19], DenseNet-121 [20], InceptionV3 [45], ViT-L16, ViT-L32 [13]}. We use 1000 ImageNet-like RGB images from the NeurIPS-17 challenge [2]. The dataset has 1000 classes same as ImageNet and all images in size  $224 \times 224$ .

**Attack settings.** We only focus on targeted attacks since they are more challenging than untargeted attacks and align with our transformation-dependent attacks formulation. We consider three transform parameters  $\{\theta_i\}_{i=1}^3$  and our goal is to deceive the model into providing three distinct desired target labels when the victim model is provided with corresponding transformed versions of perturbed images. We randomly select three unique target labels  $\{y_i^*\}_{i=1}^3$  from 1k ImageNet classes that are different from the image ground-truth label. We use  $\ell_{\infty}$  norm bound, with visually imperceptible perturbation budget  $\|\delta\|_{\infty} \leq 10$  for experiments presenting scale dependent attacks in Sec. 4.2.

**Evaluation metrics.** We evaluate the transform-dependent attack performance using the Attack Success Rate (ASR). Specifically, for a perturbed image transformed as  $T(\mathbf{x} + \delta; \theta_i)$ , we check whether the network prediction matches target label  $y_i^*$ . We report ASR for each transform parameter  $\theta_i$  and the average ASR over all three parameters.

### 4.2. Transformation-dependent attacks

We present our transformation-dependent attacks on a variety of transformation techniques that we select according to potential applications in real world scenarios. On selection of different transformations for experiments, we select a broad range of transformations including geometric



(e.g., scaling, blurring), photometric transformations (e.g., Gamma correction) and image compression (e.g. JPEG). For each transformation, we predefined transformation parameters  $\{\theta_i\}_{i=1}^3$  with the principle that the transformation has the minimum impact on model accuracy. We then evaluate ASR (%) on transformation-dependent adversarial examples. For reference, we also provide classification accuracy (ACC) evaluation on clean images under same transformations in the supplementary.

**Scale-dependent attack.** Considering real-world cases, images can be displayed at different levels of resolution, here we employ scaling transformation and create targeted attacks according to the image resolution. For the scaling, we select three transform parameters as scaling factor  $S \in \{0.5, 1.0, 1.5\}$ , at which images will be bilinearly interpolated to resolutions of  $112 \times 112$ ,  $224 \times 224$  and  $336 \times 336$ . Results in the scale-dependent attack part of Tab. 1 show perturbation effectively provides desired target labels when the transformations embedded with attacks are applied over the perturbed images.

**Blur-dependent attack.** We also employ Gaussian blur to create blur-dependent attacks, mimicking images taken in out-of-focus scenarios in the real world. We fix the Gaussian kernel size as 5 and vary standard deviation  $\sigma$  which is used for creating kernel as the transform parameter. Specifically, we choose  $\sigma \in \{0.5, 1.5, 3.0\}$  for creating small, mid and sever levels of blurry effects. Results in Tab. 1 show three targeted attacks successfully when images received the desired blurry distortions.

**Gamma-dependent attack.** Beyond linear transformations, we also consider gamma correction — a widely used technique for compensating the non-linear characteristics of display devices, also generally used for simulating lighting condition variation in DNN training. We adopt  $\gamma = \{0.5, 1.0, 2.0\}$  for simulation of bright, normal and dark lighting conditions. Their visual effects can be referred to in the second row of Fig. 1. Results in Tab. 1 demonstrate that our attacks effectively cooperate with this non-linear image transformation, and exhibit three distinct targeted attacks under three simulated lighting conditions.

**Compression-dependent attack.** We demonstrate that images compressed at different levels exhibit varying attack effects. Specifically, we consider widely used JPEG compression and implement differentiable JPEG compression, referring to [42]. For this transformation, we use compression qualities  $Q \in \{20, 50, 80\}$  as transformation parameters. Higher value of  $Q$  indicates less compression loss. Results in Tab. 1 show our attack formulation is effective with image compression.

### 4.3. Transformation-dependent attacks study

**Loss profile of transform-dependent attacks.** We take adversaries generated in Sec. 4.2 and perform a study over the

loss function Eq. (1) with respect to three transform-specific targets. In Fig. 2, we present a loss landscape generated by sweeping transformation parameters for each transform function and compute loss values over transformed adversarial examples. We observe that adversaries successfully learned to embed with transform functions at given transform parameters. Figures in the first row are computed over the surrogate model, we observe the minimum loss value occurs at the corresponding predefined parameter for each target. For reference, the second row shows the loss landscape of adversaries being forwarded to a non-surrogate model, we observe that loss curves for different targets do not exhibit a transformation-dependent pattern and present a similar trend.

**Number of transformations.** Observing that multiple targeted attacks can be embedded with image transformations in a single perturbation, a natural question raised: “*how many transformation-dependent targets can we embed in one attack?*” We conduct a study on {ResNet50, InceptionV3, ViT-L16} with scaling, blurring, gamma transformations and JPEG compression. We initialize the transform parameter schedule as  $\{0.5\}$  for scaling, blurring, gamma correction and  $\{20\}$  for JPEG compression. Gradually append new  $\theta_i$  samplings with adaptive step size to the schedule until it reach to 25 samplings at maximum. ASR vs number of samplings in Fig. 3 shows as the number of samplings increase, ASR dropping rate varied across models and transformations. Among all four transformations, scaling and JPEG have larger capacity for embedding more targeted attacks than blurring and Gamma correction. Among all three models, ResNet50 and ViT-L16 has the overall larger and smaller embedding space. We used a single NVIDIA RTX 2080Ti (12 GB) for all the experiments. Average times for generating  $\{3, 5, 10\}$  target attacks are  $\{2.61, 4.29, 8.67\}$  sec/image.

**Visual examples.** In Fig. 4 we provide examples of each image transformation we experimented with in Sec. 4.2. Examples show that our attacks can trigger various targeted attacks under a variety of image transformations while keeping good imperceptibility in terms of visual and network level — clean images under the same condition network provide correct predictions. Demonstrating a descent controllability and stealthiness introduced by our attack formulation.

### 4.4. Attacks against robust models

To further evaluate the effectiveness of the transformation-dependent attacks, we assess their performance on five defense methods, including models robustified with adversarial training (AT) [16], HGD [26], Randomized Smoothing (RS) [7], JPEG compression (JPEG) [18] and NPR [33].

**Attacks against robustified models.** We employ ResNet50 models adversarially trained on the ImageNet dataset

Table 1. Transformation-dependent targeted ASR (%)  $\uparrow$  of selected classification models. Higher value indicates better attack performance.

Transform parameter	Classifier model					
	VGG19	ResNet50	Dense121	Incv3	ViT-L16	ViT-L32
<i>T</i> : Scaling						
$S = 0.5$	99.50	96.80	95.60	76.70	77.60	61.70
$S = 1.0$	100.0	99.70	99.80	91.30	95.20	76.70
$S = 1.5$	100.0	99.60	99.60	84.00	91.60	71.80
Average	99.83	98.70	98.33	84.00	88.07	70.07
<i>T</i> : Blurring						
$\sigma = 0.5$	100.0	99.70	99.90	89.80	94.40	87.70
$\sigma = 1.5$	99.60	96.80	98.70	75.20	75.00	64.30
$\sigma = 3.0$	99.00	95.70	98.20	71.90	71.10	54.30
Average	99.53	97.40	98.93	78.97	80.17	68.77
<i>T</i> : Gamma						
$\gamma = 0.5$	100.0	99.90	99.80	89.40	95.30	89.50
$\gamma = 1.0$	100.0	99.90	100.0	91.70	97.90	92.40
$\gamma = 2.0$	100.0	99.80	99.90	88.50	87.80	77.50
Average	100.0	99.87	99.90	89.87	93.67	86.47
<i>T</i> : JPEG						
$Q = 20$	95.90	89.40	88.40	72.00	65.70	72.40
$Q = 50$	99.40	96.00	97.80	83.20	83.10	82.00
$Q = 80$	99.30	98.70	98.90	86.50	87.50	80.60
Average	98.19	94.70	95.03	80.57	78.77	78.33

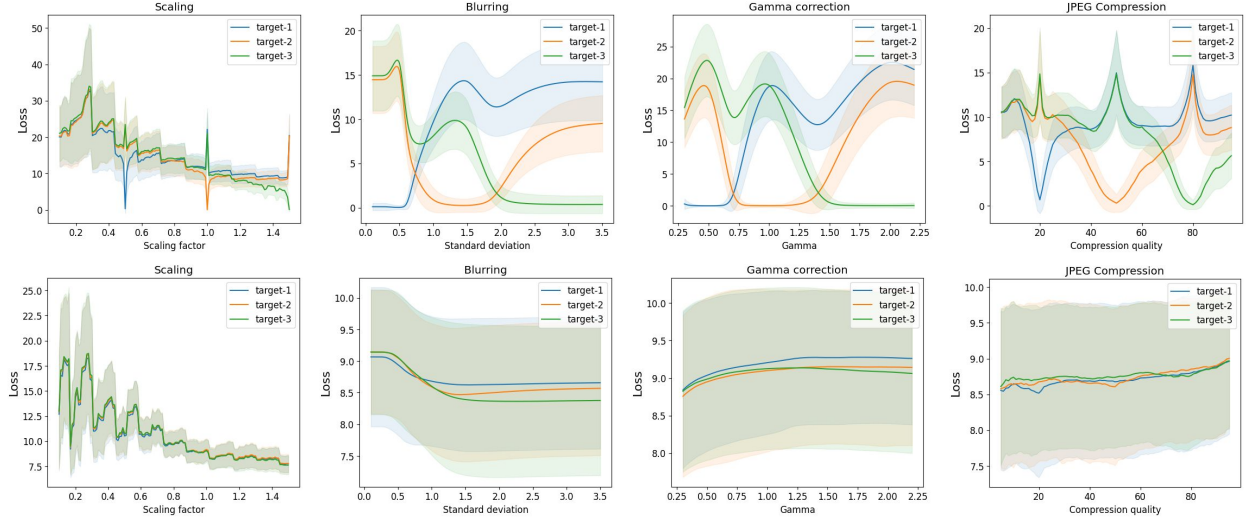


Figure 2. Loss landscape visualization. Three targeted attacks are optimized to be triggered for three transformation parameters. *i.e.*,  $S = \{0.5, 1.0, 1.5\}$ ,  $\sigma = \{0.5, 1.5, 3.0\}$ ,  $\gamma = \{0.5, 1.0, 2.0\}$ ,  $Q = \{20, 50, 80\}$  for scaling, blurring, gamma correction and JPEG compression respectively. The first and the second rows are loss landscapes on models that are used and not used for generating transformation-dependent attacks. Variation of each curve is shaded.

from [14]. Specifically, we select pre-trained models robustly against  $\ell_\infty \leq 4, 8$  untargeted attack adversaries. These models are robust in the way that they can provide consistent predictions for perturbed images to the clean images, *i.e.* model consistency defined as  $f(\mathbf{x}^*) = f(\mathbf{x})$ .

To ensure fairness in evaluation, here we adjust pertur-

bation budget according to model adversarial training settings, *i.e.*  $\varepsilon = 4, 8$  for attacking ResNet50-eps4,8 in Tab. 2. We formulate attack plans to deviate the model predictions, *i.e.* lowering model consistency, and use untargeted-like ASR metric that if the model fails to provide consistent predictions for images with and without transformations, then

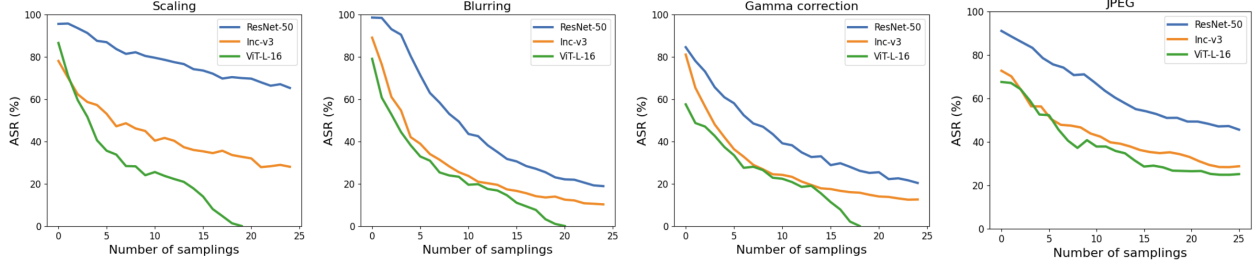


Figure 3. Average attack success rate vs the number of samplings across scaling, blurring, gamma correction, and JPEG compression. As the number of targeted attacks increases, the ASR drop indicates that the attack becomes more challenging.

Table 2. Results of attacking adversarial-robust models with transformation-dependent attacks. We use perturbation budget  $\varepsilon = \{10, 4, 8\}$  for attacking  $\{\text{ResNet50}, \text{ResNet50-eps4}, \text{ResNet50-eps8}\}$  respectively. We report model consistency (%) and ASR (%)  $\uparrow$  for adversarially perturbed images at *Original* and *Transformed* conditions respectively.

Model	Scaling			Blurring		
	Original	Transformed		Original	Transformed	
	$S = 1.0$	$S = 0.5$	$S = 1.5$	-	$\sigma = 0.5$	$\sigma = 1.5$
ResNet50	94.00	99.67	100.0	0.0	100.0	99.67
ResNet50-eps4	87.67	67.33	53.17	76.00	29.33	57.67
ResNet50-eps8	82.00	79.00	49.00	65.00	40.00	61.67
Average	87.89	82.00	67.39	47.00	56.44	73.03

Model	Gamma correction			JPEG compression		
	Original	Transformed		Original	Transformed	
	$\gamma = 1.0$	$\gamma = 0.5$	$\gamma = 2.0$	$Q = 100$	$Q = 50$	$Q = 80$
ResNet50	9.00	100.0	100.0	74.37	98.67	99.67
ResNet50-eps4	99.33	61.67	69.33	81.67	48.67	46.67
ResNet50-eps8	99.33	66.0	75.00	75.00	52.33	50.78
Average	69.22	75.89	81.44	77.01	66.56	65.71

the attacks are considered successful. *i.e.*  $f(T(\mathbf{x}^*; \theta)) \neq f(\mathbf{x}^*)$ . Our attack plan formulated using transform parameters  $S = \{0.5, 1.5\}$ ,  $\sigma = \{0.5, 1.5\}$ ,  $\gamma = \{0.5, 2.0\}$  and  $Q = \{50, 100\}$  with 2 randomly select targets.

Results in Tab. 2 show our attacks effectively disrupt the robustified models in the transformation space that for image under the original condition (*e.g.*, when  $S = 1.0$ ,  $\gamma = 1.0$ ,  $Q = 100$  and no blurring) the prediction consistency of robust models are not affected by transform-dependent perturbation, *i.e.*  $f(\mathbf{x}^*) = f(\mathbf{x})$ . However, after applying transform functions, models fail to provide consistent predictions as perturbed images under the original condition, *i.e.*  $f(T(\mathbf{x}^*; \theta)) \neq f(\mathbf{x}^*)$ . For reference, we provide model consistency evaluation of experimental models on clean images  $f(T(\mathbf{x}; \theta)) = f(\mathbf{x})$  in the supplementary.

**Evaluations on other defense methods.** Following the settings in one of the recent transfer-based methods BPA [52], we evaluated the performance of untargted attacks against four defenses applied to the surrogate model. We use the ground-truth label ( $y$ ) as the target in Eq. (4) for all transform parameters  $\theta_i$  and maximize the loss as untargted at-

tacks in our attack optimization. In Tab. 3, we report the untargted ASRs averaged over all the transform parameters. For a fair comparison with BPA methods, we used  $\varepsilon = 8$  in these experiments, and our attack archives overall better performance than BPA on the same benchmark. These results suggest that transform-dependent attacks can bypass existing defense methods by leveraging the transformation space beyond adversarial-robust models evaluated in Tab. 2.

Table 3. Untargted ASR (%)  $\uparrow$  against defense methods,  $\varepsilon = 8$

Attack method	Defense method			
	HGD [26]	RS [7]	JPEG [18]	NPR [33]
BPA [52]	23.96	14.00	22.52	14.08
Scaling (ours)	56.20	53.43	34.90	39.70
Blurring(ours)	57.73	63.67	57.80	52.43
Gamma(ours)	48.67	65.43	52.27	53.57

#### 4.5. Transfer attacks against blackbox models

In this section, we evaluate the transfer success rate of our attacks on blackbox models.

Instead of generating attacks for a fixed scaling factor  $S$  and blurring  $\sigma$  as in Sec. 4.2 (*i.e.*  $S = \{0.5, 1.0, 1.5\}$  and  $\sigma = \{0.5, 1.5, 3.0\}$ ), in this experiment we gen-



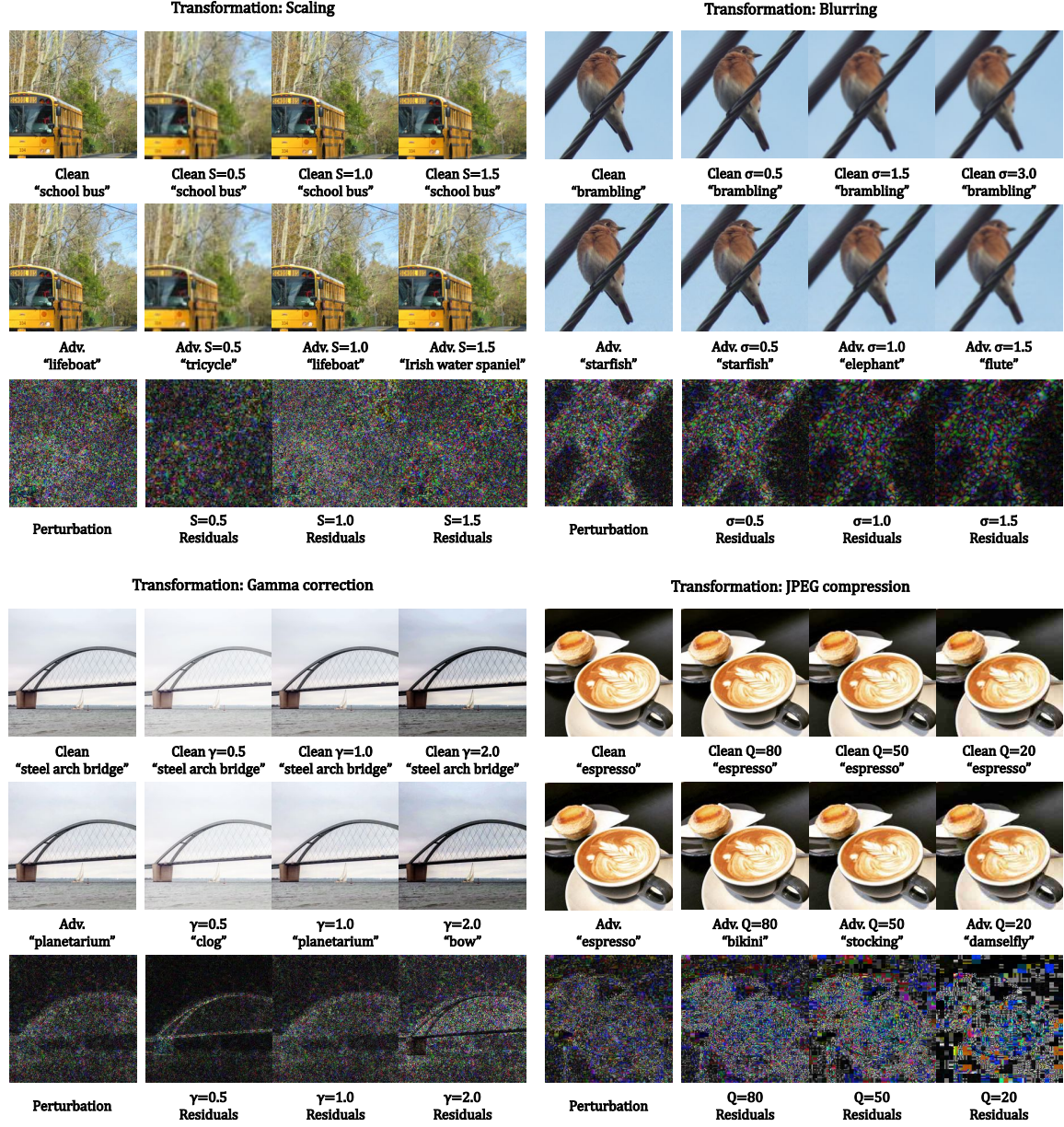


Figure 4. We provide predictions for clean and perturbed (Adv.) images under each transformation with different parameters. For display, images under scaling are originally in resolutions of  $\{112, 224, 336\}$  for  $S = \{0.5, 1.0, 1.5\}$  and are resized to 224; the magnitude of residuals (*i.e.*  $T(\mathbf{x}; \theta) - T(\mathbf{x}^*; \theta)$ ) and perturbations is amplified by  $30\times$ .

erate attacks over a range of parameters  $S$  and  $\sigma$  (*i.e.*  $S \sim \{[0.4, 0.6], [0.9, 1.1], [1.4, 1.6]\}$  and  $\sigma \sim \{[0.4, 0.6], [1.4, 1.6], [2.9, 3.1]\}$ ), which can contribute to transfer attack success according to [1].

We provide the evaluation of blackbox transfer of our attacks in untargeted and targeted settings in Tab. 4.

Our method achieves untargeted/targeted ASRs comparable to recent transfer-based methods [25, 50, 52] without any special adaptation.

Note that most of the existing transfer-based methods report impressive results only for untargeted attacks. The transfer ASR for targeted attacks remains quite low in a small perturbation budget. For reference, we include results from BPA [52], ILPD [25] and SU [50] with the same dataset, surrogate models (ResNet50), and target labels.

For a fair and comprehensive comparison with these methods, we used  $\varepsilon = 8$  and introduced the model MobileNet-v2 [40] in these experiments.

Table 4. Blackbox transfer evaluation, perturbation budget  $\varepsilon = 8$ .

Methods	Surrogate	Blackbox			
	ResNet50	VGG19	Dense121	Incv3	Mobv2
Untargeted ASR (%) $\uparrow$					
BPA [52]	99.40	60.96	70.70	35.36	68.90
ILPD [25]	83.96	<b>88.10</b>	<b>90.68</b>	64.70	-
$S \sim [0.4, 0.6]$	88.00	80.10	81.10	<b>96.90</b>	<b>86.80</b>
$S \sim [0.9, 1.1]$	98.30	86.70	77.50	62.60	81.00
$S \sim [1.4, 1.6]$	99.90	85.40	83.90	58.90	85.10
$\sigma \sim [0.4, 0.6]$	99.80	64.40	69.40	53.50	65.60
$\sigma \sim [1.4, 1.6]$	99.80	85.40	84.60	73.70	83.80
$\sigma \sim [2.9, 3.1]$	99.60	86.80	85.50	76.30	85.00
Targeted ASR (%) $\uparrow$					
BPA [52]	100.0	31.02	43.82	15.34	39.00
Logit-SU [50]	-	41.30	45.70	1.10	-
$S \sim [0.4, 0.6]$	99.60	39.10	40.00	12.10	31.50
$S \sim [0.9, 1.1]$	99.90	<b>62.80</b>	61.40	28.80	56.10
$S \sim [1.4, 1.6]$	100.0	59.50	<b>67.80</b>	<b>33.10</b>	<b>60.00</b>
$\sigma \sim [0.4, 0.6]$	100.0	32.60	42.20	19.10	35.00
$\sigma \sim [1.4, 1.6]$	99.90	43.90	52.60	23.40	35.40
$\sigma \sim [2.9, 3.1]$	99.90	41.90	50.40	22.50	33.80

#### 4.6. Extension to object detection task

**Models and dataset.** For the object detection task, we utilize detector models pretrained on COCO 2017 dataset [28] from MMDetection [6]. Specifically, we select two one-stage models {YOLOv3 [37], FCOS [46]}, two two-stage models {Faster R-CNN [38], Grid R-CNN [29]} and one ViT-based model DETR [3]. For dataset, we use 500 images from COCO 2017 validation that contain objects in 3 unique categories denoted as  $A$ ,  $B$  and  $C$ .

**Attack scenario and evaluation.** We consider scaling transformation out of the simplicity and consistency with previous experiments and continue with the same scaling factors  $S \in \{0.5, 1.0, 1.5\}$  and try to achieve attack effects namely scale selective hiding. Our objective is to conceal objects belonging to one of the categories from  $A$ ,  $B$ , and  $C$  in the detection results of  $T(\mathbf{x}; 0.5)$ ,  $T(\mathbf{x}; 1.0)$  and  $T(\mathbf{x}; 1.5)$ , *i.e.* hide all  $A$  objects when image scaling to  $0.5\times$ , hide all  $B$ s when scaling to  $1.0\times$  and hide all  $C$ s when scaling to  $1.5\times$ .

In this scenario, we measure ASR as *the ratio of successfully hidden objects in the final detection result* of the corresponding scaled input image.

**Results and visualization.** Tab. 5 show that over most R-CNN-based detectors, the scale-dependent attack effects are successfully triggered when adversaries scale to the corresponding image size. In Fig. 5, we provide a successful example of selective hiding effects and utilize the Grad-CAM [41] to visualize the feature level understanding of the detector. Our results show that transform-dependent attacks can be extended to more complex dense prediction models.

## 5. Discussion

To the best of our knowledge, this is the first work to demonstrate that a single (imperceptible) adversarial perturbation can be used to trigger transform-dependent (controllable) attacks. The idea is simple but reveals new and intriguing

properties of adversarial attacks and vulnerable spaces in deep networks. For instance, this method can be viewed as a simple alternative to backdoor attacks. But unlike standard backdoor attacks [17, 54], which require to attack in the way that training a backdoor model with malicious triggers, instead, we add a single perturbation that with image transformations can trigger (desired) responses from the models. **Limitations.** While our work provides important empirical demonstrations of transformation-dependent adversarial attacks across various settings, there remain several limitations that warrant further investigation. Firstly, although we observe the effectiveness of these attacks in inducing diverse misclassifications through input transformations, the underlying mechanisms by which the adversarial perturbations interact with and manipulate the transformations to change network behavior are not fully clear. A deeper feature-level study is needed to understand how different transformations modify the input content or frequency components in ways that can be exploited adversarially. Secondly, while we showcase real-world implications through the object detection task, the deployment of such transformation-dependent attacks in physical environments and their effectiveness under real-world conditions requires more extensive evaluation.

**Future directions.** Based on the limitations of this work, we identify several future directions, including feature-level analysis to gain insights into how image transformations introduce or modify content properties that enable adversarial manipulation when combined with carefully crafted perturbations. Additionally, extending the transformation-dependent formulation to patch-based attacks tailored for physical environments, where localized adversarial patterns can induce diverse effects by transforming the camera viewpoint or object pose, rotations, and locations, is another promising direction. Our proposed attack generates a “static/fixed” perturbation that can trigger “dynamic/controllable” adversarial effects in real-time deployment. While the computational cost for generating such adversarial perturbations is proportional to the number of attacks (as evidenced in Sec. 4.3), different attacks can be deployed or changed with minimal cost through simple transformations. For instance, in surveillance systems or facial authentication, an attacker could hide or impersonate a person by simply transforming the input image. In principle, this method can be extended to physical attacks where attackers manipulate objects through simple transformations like scaling and rotating to achieve different effects. For example, an object can be made to appear, disappear, or be misclassified based on distance or blur.

## 6. Conclusion

This work unveils transformation-dependent adversarial attacks, a formidable new threat where carefully crafted per-



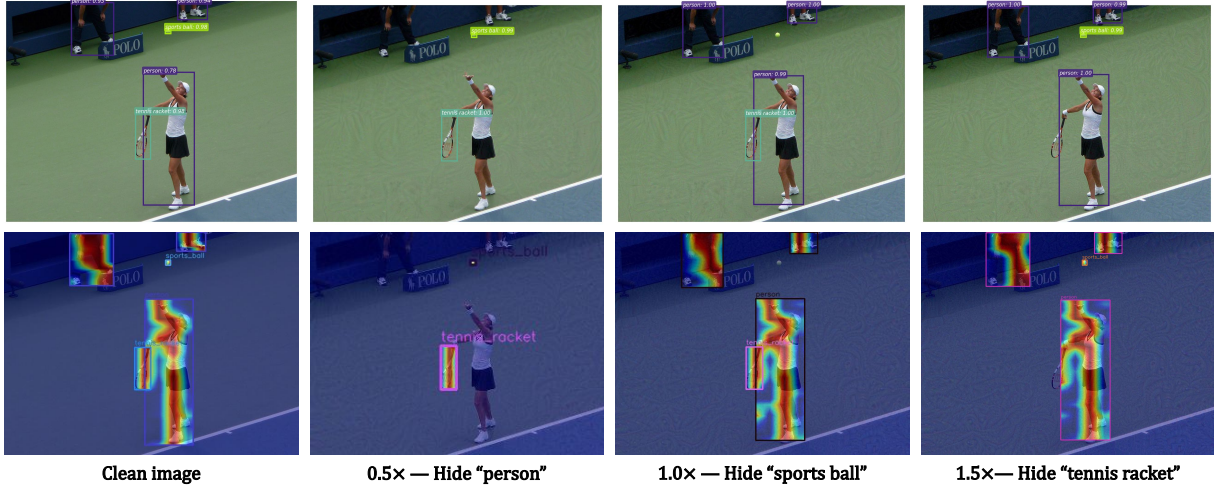


Figure 5. Visualization of scale-dependent selective hiding attack against YOLOv3. The first row is the detection results of YOLOv3 on clean image and  $\{0.5, 1.0, 1.5\} \times$  adversaries. ImageID: 000000037988.

Table 5. Scale-dependent selective hiding attack success rate (ASR) over object detection models. ASRs are reported at each target scaling factor and average over all factors. Higher value indicates better attack performance.

Scaling factor	Detector model ASR (%) $\uparrow$ $\ \delta\ _{\infty} \leq 10$					Detector model ASR (%) $\uparrow$ $\ \delta\ _{\infty} \leq 20$				
	Faster	YOLOv3	FCOS	GRID	DETR	Faster	YOLOv3	FCOS	GRID	DETR
$S = 0.5$	53.85	97.39	71.61	54.44	11.91	60.26	97.39	76.39	67.22	17.16
$S = 1.0$	65.71	95.10	69.38	58.89	11.95	72.76	98.04	79.26	68.52	23.61
$S = 1.5$	90.71	32.35	100.0	86.11	41.26	96.15	40.98	100.0	97.78	52.18
Average	70.09	74.95	80.33	66.48	21.71	76.39	78.80	85.22	77.84	30.98

turbations can induce a wide variety of targeted misclassifications by dynamically transforming the input. Our extensive experiments across diverse models and tasks demonstrate the remarkable vulnerability of deep networks to manifest controllable attack effects from a single perturbation. These attacks shatter the traditional notion of adversarial inputs being static, isolated instances - their adversarial nature is now a complex, chameleon-like capability to react differently under transformations. This work calls for a necessary paradigm shift in how we understand and defend against adversarial threats in machine learning.

**Acknowledgments.** This material is based upon work supported by AFOSR award FA9550-21-1-0330, NSF award 2046293, and UC Regents Faculty Development grant.

## References

- [1] Anish Athalye, Logan Engstrom, Andrew Ilyas, and Kevin Kwok. Synthesizing robust adversarial examples. In *International conference on machine learning*, pages 284–293. PMLR, 2018. 1, 3, 8
- [2] Google Brain. Neurips 2017: Targeted adversarial attack. <https://www.kaggle.com/competitions/nips-2017-targeted-adversarial-attack/data>, 2017. [On Kaggle]. 4
- [3] Nicolas Carion, Francisco Massa, Gabriel Synnaeve, Nicolas Usunier, Alexander Kirillov, and Sergey Zagoruyko. End-to-end object detection with transformers. In *European conference on computer vision*, pages 213–229. Springer, 2020. 9
- [4] Nicholas Carlini and David Wagner. Towards evaluating the robustness of neural networks. In *2017 IEEE Symposium on Security and Privacy (SP)*, pages 39–57. IEEE, 2017. 13
- [5] Jiyu Chen, David Wang, and Hao Chen. Explore the transformation space for adversarial images. In *Proceedings of the Tenth ACM Conference on Data and Application Security and Privacy*, pages 109–120, 2020. 3
- [6] Kai Chen, Jiaqi Wang, Jiangmiao Pang, Yuhang Cao, Yu Xiong, Xiaoxiao Li, Shuyang Sun, Wansen Feng, Ziwei Liu, Jiarui Xu, Zheng Zhang, Dazhi Cheng, Chenchen Zhu, Tianheng Cheng, Qijie Zhao, Buyu Li, Xin Lu, Rui Zhu, Yue Wu, Jifeng Dai, Jingdong Wang, Jianping Shi, Wanli Ouyang, Chen Change Loy, and Dahua Lin. MMDetection: Open mmlab detection toolbox and benchmark. *arXiv preprint arXiv:1906.07155*, 2019. 9
- [7] Jeremy Cohen, Elan Rosenfeld, and Zico Kolter. Certified adversarial robustness via randomized smoothing. In *international conference on machine learning*, pages 1310–1320. PMLR, 2019. 5, 7



- [8] Francesco Croce and Matthias Hein. Reliable evaluation of adversarial robustness with an ensemble of diverse parameter-free attacks. In *ICML*, 2020. 3
- [9] Francesco Croce and Matthias Hein. Mind the box:  $l_1$ -apgd for sparse adversarial attacks on image classifiers. In *ICML*, 2021. 3
- [10] Jia Deng, Wei Dong, Richard Socher, Li-Jia Li, Kai Li, and Li Fei-Fei. Imagenet: A large-scale hierarchical image database. In *2009 IEEE conference on computer vision and pattern recognition*, pages 248–255. IEEE, 2009. 4
- [11] Yinpeng Dong, Fangzhou Liao, Tianyu Pang, Hang Su, Jun Zhu, Xiaolin Hu, and Jianguo Li. Boosting Adversarial Attacks with Momentum. In *Proceedings of the IEEE conference on computer vision and pattern recognition*, pages 9185–9193, 2018. 1, 3, 13
- [12] Yinpeng Dong, Tianyu Pang, Hang Su, and Jun Zhu. Evading defenses to transferable adversarial examples by translation-invariant attacks. In *Proceedings of the IEEE/CVF Conference on Computer Vision and Pattern Recognition*, pages 4312–4321, 2019. 1, 3
- [13] Alexey Dosovitskiy, Lucas Beyer, Alexander Kolesnikov, Dirk Weissenborn, Xiaohua Zhai, Thomas Unterthiner, Mostafa Dehghani, Matthias Minderer, Georg Heigold, Sylvain Gelly, et al. An image is worth 16x16 words: Transformers for image recognition at scale. In *International Conference on Learning Representations*, 2020. 4
- [14] Logan Engstrom, Andrew Ilyas, Hadi Salman, Shibani Santurkar, and Dimitris Tsipras. Robustness (python library), 2019. 6
- [15] Logan Engstrom, Brandon Tran, Dimitris Tsipras, Ludwig Schmidt, and Aleksander Madry. Exploring the landscape of spatial robustness. In *International conference on machine learning*, pages 1802–1811. PMLR, 2019. 3
- [16] Ian J Goodfellow, Jonathon Shlens, and Christian Szegedy. Explaining and harnessing adversarial examples. In *International Conference on Learning Representations*, 2015. 1, 3, 5, 13
- [17] Tianyu Gu, Kang Liu, Brendan Dolan-Gavitt, and Siddharth Garg. Badnets: Evaluating backdooring attacks on deep neural networks. *IEEE Access*, 7:47230–47244, 2019. 9
- [18] Chuan Guo, Mayank Rana, Moustapha Cisse, and Laurens Van Der Maaten. Countering adversarial images using input transformations. 2018. 5, 7
- [19] Kaiming He, Xiangyu Zhang, Shaoqing Ren, and Jian Sun. Deep residual learning for image recognition. In *Proceedings of the IEEE conference on computer vision and pattern recognition*, pages 770–778, 2016. 4
- [20] Gao Huang, Zhuang Liu, Laurens Van Der Maaten, and Kilian Q Weinberger. Densely connected convolutional networks. In *Proceedings of the IEEE conference on computer vision and pattern recognition*, pages 4700–4708, 2017. 4
- [21] Max Jaderberg, Karen Simonyan, Andrew Zisserman, et al. Spatial transformer networks. *Advances in neural information processing systems*, 28, 2015. 3, 4
- [22] Alexey Kurakin, Ian Goodfellow, and Samy Bengio. Adversarial examples in the physical world. *arXiv preprint arXiv:1607.02533*, 2016. 1
- [23] Alexey Kurakin, Ian J Goodfellow, and Samy Bengio. Adversarial examples in the physical world. In *Artificial intelligence safety and security*, pages 99–112. Chapman and Hall/CRC, 2018. 3
- [24] Max Lennon, Nathan Drenkow, and Phil Burlina. Patch attack invariance: How sensitive are patch attacks to 3d pose? In *Proceedings of the IEEE/CVF International Conference on Computer Vision (ICCV) Workshops*, pages 112–121, 2021. 3
- [25] Qizhang Li, Yiwen Guo, Wangmeng Zuo, and Hao Chen. Improving adversarial transferability via intermediate-level perturbation decay. *Advances in Neural Information Processing Systems*, 36, 2024. 8, 9
- [26] Fangzhou Liao, Ming Liang, Yinpeng Dong, Tianyu Pang, Xiaolin Hu, and Jun Zhu. Defense against adversarial attacks using high-level representation guided denoiser. In *Proceedings of the IEEE conference on computer vision and pattern recognition*, pages 1778–1787, 2018. 5, 7
- [27] Jiadong Lin, Chuanbiao Song, Kun He, Liwei Wang, and John E. Hopcroft. Nesterov accelerated gradient and scale invariance for adversarial attacks. In *8th International Conference on Learning Representations, ICLR 2020, Addis Ababa, Ethiopia, April 26-30, 2020*, 2020. 1, 3
- [28] Tsung-Yi Lin, Michael Maire, Serge Belongie, James Hays, Pietro Perona, Deva Ramanan, Piotr Dollár, and C Lawrence Zitnick. Microsoft coco: Common objects in context. In *European conference on computer vision*, pages 740–755. Springer, 2014. 9
- [29] Xin Lu, Buyu Li, Yuxin Yue, Quanguan Li, and Junjie Yan. Grid r-cnn. In *Proceedings of the IEEE/CVF Conference on Computer Vision and Pattern Recognition*, pages 7363–7372, 2019. 9
- [30] Aleksander Madry, Aleksandar Makelov, Ludwig Schmidt, Dimitris Tsipras, and Adrian Vladu. Towards deep learning models resistant to adversarial attacks. In *International Conference on Learning Representations*, 2018. 1, 3, 13
- [31] Diego Marcos, Michele Volpi, Nikos Komodakis, and Devis Tuia. Rotation equivariant vector field networks. In *Proceedings of the IEEE International Conference on Computer Vision*, pages 5048–5057, 2017. 4
- [32] Seyed-Mohsen Moosavi-Dezfooli, Alhussein Fawzi, Omar Fawzi, and Pascal Frossard. Universal adversarial perturbations. In *Proceedings of the IEEE conference on computer vision and pattern recognition*, pages 1765–1773, 2017. 2
- [33] Muzammal Naseer, Salman Khan, Munawar Hayat, Fahad Shahbaz Khan, and Fatih Porikli. A self-supervised approach for adversarial robustness. In *Proceedings of the IEEE/CVF Conference on Computer Vision and Pattern Recognition*, pages 262–271, 2020. 5, 7
- [34] Nicolas Papernot, Patrick McDaniel, Ian Goodfellow, Somesh Jha, Z Berkay Celik, and Ananthram Swami. Practical black-box attacks against machine learning. In *Proceedings of the 2017 ACM on Asia conference on computer and communications security*, pages 506–519, 2017. 2
- [35] Adam Paszke, Sam Gross, Soumith Chintala, Gregory Chanan, Edward Yang, Zachary DeVito, Zeming Lin, Alban Desmaison, Luca Antiga, and Adam Lerer. Automatic differentiation in pytorch. 2017. 4

- [36] Kexin Pei, Linjie Zhu, Yinzhi Cao, Junfeng Yang, Carl Vondrick, and Suman Jana. Towards practical verification of machine learning: The case of computer vision systems. *arXiv preprint arXiv:1712.01785*, 2017. 3
- [37] Joseph Redmon and Ali Farhadi. Yolov3: An incremental improvement. *arXiv preprint arXiv:1804.02767*, 2018. 9
- [38] Shaoqing Ren, Kaiming He, Ross Girshick, and Jian Sun. Faster r-cnn: Towards real-time object detection with region proposal networks. In *Advances in neural information processing systems*, pages 91–99, 2015. 9
- [39] Henry A Rowley, Shumeet Baluja, and Takeo Kanade. Rotation invariant neural network-based face detection. In *Proceedings. 1998 IEEE computer society conference on computer vision and pattern recognition (Cat. No. 98CB36231)*, pages 38–44. IEEE, 1998. 4
- [40] Mark Sandler, Andrew Howard, Menglong Zhu, Andrey Zhmoginov, and Liang-Chieh Chen. Mobilenetv2: Inverted residuals and linear bottlenecks. In *Proceedings of the IEEE conference on computer vision and pattern recognition*, pages 4510–4520, 2018. 8
- [41] Ramprasaath R Selvaraju, Michael Cogswell, Abhishek Das, Ramakrishna Vedantam, Devi Parikh, and Dhruv Batra. Grad-cam: Visual explanations from deep networks via gradient-based localization. In *Proceedings of the IEEE international conference on computer vision*, pages 618–626, 2017. 9
- [42] Richard Shin and Dawn Song. Jpeg-resistant adversarial images. In *NIPS 2017 Workshop on Machine Learning and Computer Security*, page 8, 2017. 3, 5
- [43] Karen Simonyan and Andrew Zisserman. Very deep convolutional networks for large-scale image recognition. *arXiv preprint arXiv:1409.1556*, 2014. 4
- [44] Christian Szegedy, Wojciech Zaremba, Ilya Sutskever, Joan Bruna, Dumitru Erhan, Ian Goodfellow, and Rob Fergus. Intriguing properties of neural networks. In *International Conference on Learning Representations*, 2014. 3
- [45] Christian Szegedy, Vincent Vanhoucke, Sergey Ioffe, Jon Shlens, and Zbigniew Wojna. Rethinking the inception architecture for computer vision. In *Proceedings of the IEEE conference on computer vision and pattern recognition*, pages 2818–2826, 2016. 4
- [46] Zhi Tian, Chunhua Shen, Hao Chen, and Tong He. Fcos: Fully convolutional one-stage object detection. In *Proceedings of the IEEE/CVF international conference on computer vision*, pages 9627–9636, 2019. 9
- [47] Florian Tramèr, Alexey Kurakin, Nicolas Papernot, Ian Goodfellow, Dan Boneh, and Patrick McDaniel. Ensemble adversarial training: Attacks and defenses. *arXiv preprint arXiv:1705.07204*, 2017. 2
- [48] Xiaosen Wang, Xuanran He, Jingdong Wang, and Kun He. Admix: Enhancing the transferability of adversarial attacks. In *Proceedings of the IEEE/CVF International Conference on Computer Vision*, pages 16158–16167, 2021. 1, 3
- [49] Xiaosen Wang, Zeliang Zhang, and Jianping Zhang. Structure invariant transformation for better adversarial transferability. In *Proceedings of the IEEE/CVF International Conference on Computer Vision*, pages 4607–4619, 2023. 1, 3
- [50] Zhipeng Wei, Jingjing Chen, Zuxuan Wu, and Yu-Gang Jiang. Enhancing the self-universality for transferable targeted attacks. In *Proceedings of the IEEE/CVF conference on computer vision and pattern recognition*, pages 12281–12290, 2023. 8, 9
- [51] Chaowei Xiao, Jun-Yan Zhu, Bo Li, Warren He, Mingyan Liu, and Dawn Song. Spatially transformed adversarial examples. In *International Conference on Learning Representations*, 2018. 3
- [52] Wang Xiaosen, Kangheng Tong, and Kun He. Rethinking the backward propagation for adversarial transferability. *Advances in Neural Information Processing Systems*, 36:1905–1922, 2023. 7, 8, 9
- [53] Cihang Xie, Zhishuai Zhang, Yuyin Zhou, Song Bai, Jianyu Wang, Zhou Ren, and Alan L Yuille. Improving transferability of adversarial examples with input diversity. In *Proceedings of the IEEE/CVF conference on computer vision and pattern recognition*, pages 2730–2739, 2019. 1, 3
- [54] Tong Xu, Yiming Li, Yong Jiang, and Shu-Tao Xia. Batt: Backdoor attack with transformation-based triggers. In *ICASSP 2023-2023 IEEE International Conference on Acoustics, Speech and Signal Processing (ICASSP)*, pages 1–5. IEEE, 2023. 9
- [55] Junhua Zou, Zhisong Pan, Junyang Qiu, Xin Liu, Ting Rui, and Wei Li. Improving the transferability of adversarial examples with resized-diverse-inputs, diversity-ensemble and region fitting. In *European Conference on Computer Vision*, pages 563–579. Springer, 2020. 1, 3

# Transformation-Dependent Adversarial Attacks (Supplementary Material)

## Summary

In this supplementary material, we present additional evaluation results for various models (both original and robustified) with images subjected to diverse transformations (corresponding to Sec. 4.2 and Sec. 4.4 in the main paper). We also present additional results demonstrating the efficacy of our attacks against adversarial training. Moreover, we illustrate the adaptability of our attacks to different transformation types, accompanied by additional evaluations in more challenging attack scenarios. Lastly, we include supplementary visualizations of adversarial examples to facilitate qualitative assessment.

## S1. Accuracy evaluations

In Sec. 4.2 of our main paper, we presented targeted attacks crafted to exploit vulnerabilities specific to scaling, blurring, gamma correction, and JPEG compression transformations. We assess the Attack Success Rate (ASR) on a wide range of models: {VGG-19-BN, ResNet50, DenseNet-161, InceptionV3, ViT-L-16, ViT-L-32}. Our objective here is to clarify that the adversarial effects we observe are not merely the result of image transformations but are indicative of deeper vulnerabilities introduced by our adversarial perturbations. Tab. S1 provides model classification accuracy for clean images that have undergone the same transformations we employ in our attack generation process. This comparison reveals varying degrees of sensitivity among the models to different transformations. Interestingly, while most models demonstrate robust performance (e.g., over 80% accuracy) on transformed but clean images, older architectures like InceptionV3 show a marked vulnerability. Specifically, the accuracy for InceptionV3 drops significantly to 69.70% under these conditions, highlighting a comparative lack of robustness to transformations. Our experiment underscores the evolving nature of model robustness, where newer architectures like ViT-L-16 and ViT-L-32 manage to maintain high accuracy despite transformations that significantly impact older models like VGG and InceptionV3. Nevertheless, all models are highly vulnerable to our transformation-dependent attacks.

## S2. Attacks against robust models

In Sec. 4.4 of the main paper, we demonstrate the effectiveness of transformation-dependent attacks in deceiving adversarially-trained robust models. Here, we extend our analysis by providing comprehensive evaluations for such robust models.

In addition to the experiments detailed in Table 5, which underscore the susceptibility of robust models to misclassifications induced by our attacks, we delve deeper into their performance under various transformations, as outlined in Tab. S2. Given that robustified models exhibit diminished accuracy even on clean images, our focus shifts to evaluating the “consistency” of predictions

before and after transformations. Specifically, we assess consistency by examining whether instances satisfy  $f(\mathbf{x}) = f(T(\mathbf{x}; \theta))$ .

Each column labeled *Transformed* in Tab. S2 reports the prediction consistency of images in their original form (i.e., the percentage of times  $f(\mathbf{x}) = f(T(\mathbf{x}; \theta))$ ). Notably, all values for columns labeled *Original* are 100% since the prediction for an image without any transformation remains identical to the original condition. However, in the *Transformed* columns, we observe that the non-robust ResNet50 exhibits greater resilience to distribution shift introduced by image transformations compared to ResNet50-eps4 and ResNet50-eps8.

For reference, we include a model consistency evaluation for both clean and perturbed images under the original condition (i.e., without any transformation involved in the attack) in Tab. S3. Notably, while facing attacks, the non-robust ResNet50 fails to provide consistent predictions, whereas robust models maintain consistent predictions with a consistency rate exceeding 80% on average.

Our findings underscore that traditional adversarial training falls short in effectively countering our attacks, as it entails a trade-off between in-distribution adversarial robustness and out-of-distribution generalization to transformed images.

## S3. Adapt other optimization methods

In experiments of our main paper, we mainly focus on solving transformation-dependent attacks using PGD [30]. In principle, our attacks can also be generated with other optimization methods. Here we provide results of transformation-dependent attacks adaptation with some commonly used methods, including FGSM [16], MIM [11], C&W [4], and make a comparison to PGD results presented in the main text experiment.

We present the average ASR for scale-dependent targeted attacks (under same setting as Tab. 1 in main text) in Tab. S4. MIM, C&W, and PGD are iterative methods and offer high ASR but the single-step FGSM is insufficient to solve transformation-dependent attacks.

## S4. More transformations

In addition to the transformations demonstrated in the main paper, Sec. 4.1 (scaling, blurring, gamma, and JPEG), we extend transformation-dependent attacks to two more geometric transformations — flipping and perspective transformations.

### S4.1. Flip-dependent attack

In our examination of flip-dependent attacks, we explore three specific targeted scenarios designed to activate upon the network’s receipt of images subjected to vertical flip, horizontal flip, and no flip



Table S1. Clean accuracy (ACC) evaluation over selected classification models. Higher value indicating lower classification error introduced by the image transformation.

Transform parameter	Classifier model ACC (%)					
	VGG19	ResNet50	Dense-121	Incv3	ViT-L16	ViT-L32
Scaling						
$S = 0.5$	66.00	69.20	62.20	29.30	89.10	83.00
$S = 1.0$	100.0	100.0	100.0	100.0	100.0	100.0
$S = 1.5$	87.80	90.40	92.00	79.80	97.80	96.40
Average	84.60	86.53	84.73	69.70	95.63	93.13
Blurring						
$\sigma = 0.5$	94.20	95.80	96.90	91.50	98.30	96.90
$\sigma = 1.5$	71.00	76.50	78.30	67.00	88.20	81.90
$\sigma = 3.0$	64.60	74.10	75.80	61.10	85.90	78.40
Average	76.60	82.13	83.67	73.20	90.80	85.73
Gamma						
$\gamma = 0.5$	91.90	92.30	95.80	85.00	94.40	92.70
$\gamma = 1.0$	100.0	100.0	100.0	100.0	100.0	100.0
$\gamma = 2.0$	90.90	90.70	92.80	80.60	91.80	88.60
Average	94.27	94.33	96.20	88.53	95.40	93.77
JPEG						
$Q = 20$	71.30	78.20	84.10	68.90	81.70	83.30
$Q = 50$	82.10	86.10	89.60	75.50	87.50	88.00
$Q = 80$	87.30	89.50	92.10	78.00	91.20	89.40
Average	80.23	84.60	88.60	74.13	86.80	86.90

Table S2. Robust models evaluation with only transformation. The column labeled *Original* presents model accuracy for the original images (i.e.,  $f(\mathbf{x})$ ). The column *Transformed* evaluate models accuracy after image transformations,  $f(T(\mathbf{x}; \theta))$ .

Model	Scaling			Blurring		
	Original $S = 1.0$	Transformed $S = 0.5 \quad S = 1.5$		Original -	Transformed $\sigma = 0.5 \quad \sigma = 1.5$	
ResNet-50	100.0	69.20	90.40	100.0	95.80	76.50
ResNet-50-eps4	100.0	35.40	65.20	100.0	88.10	52.90
ResNet-50-eps8	100.0	32.00	61.30	100.0	85.90	53.00
Average	100.0	45.53	72.30	100.0	89.93	60.80
Model	Gamma			JPEG		
	Original $\gamma = 1.0$	Transformed $\gamma = 0.5 \quad \gamma = 2.0$		Original $Q = 100$	Transformed $Q = 50 \quad Q = 80$	
ResNet-50	100.0	92.30	90.70	100.0	86.50	91.30
ResNet-50-eps4	100.0	43.90	35.10	100.0	88.00	91.30
ResNet-50-eps8	100.0	38.10	31.20	100.0	88.40	92.50
Average	100.0	58.10	52.33	100.0	87.63	91.70

(retaining their original orientation) as inputs. The findings, as detailed in Tab. S5, reveal a notable efficacy of these flip-dependent attacks, achieving an ASR of 90% across the majority of evaluated models.

## S4.2. Perspective-dependent attack

Here we introduce perspective-dependent attacks to mimic the variability encountered when taking photos from different angles. We categorize these variations into three predefined perspectives: viewing the subject from the front, from above, and from below, labeled as perspectives 1, 2, and 3, respectively. Specifically,

perspective 1 maintains the image in its original state, illustrating a front-facing viewpoint. Perspective 2 simulates a downward view by transforming the image axis from  $\{(0,0), (223,0)\}$  to  $\{(56,56), (168,56)\}$ , and perspective 3 simulates an upward view by altering the image axis from  $\{(0,223), (223,223)\}$  to  $\{(56,168), (168,168)\}$ .

The results, as noted in Tab. S6, demonstrate the effectiveness of these perspective-dependent attacks, with targeted strategies achieving an overall ASR of over 90% when images are presented from these varied perspectives.

Table S3. Robust models consistency rate (%). We generate attacks for each ResNet50 model and provide evaluation of models consistency rate for perturbed image without any transformation applied.

Perturbation budget	Classifier model		
	ResNet50	ResNet50-eps4	ResNet50-eps8
$\varepsilon = 4$	1.30	84.33	87.10
$\varepsilon = 8$	0.00	74.67	83.23

Table S4. Average scale-dependent ASRs (%)  $\uparrow$  with different attack optimization methods,  $\varepsilon = 10$

Attack method	ResNet50	VGG	Dense	Incv3
FGSM	0.13	0.13	0.07	0.10
C&W	86.30	90.40	89.20	60.27
MIM	98.67	99.83	98.27	<b>84.93</b>
PGD (Tab. 1 main text)	<b>98.70</b>	<b>99.83</b>	<b>98.33</b>	84.00

## S5. More challenging attack targets

In Sec. 4.2 of the main paper, we initially employed a random selection process to choose three distinct classes from the set of 1000 ImageNet classes as our target labels, denoted as  $\{y_i^*\}_{i=1}^3$ . Here, we maintain consistency with our attack settings and classification models, but instead of random selection, we opt to target the *three least-likely labels* extracted from the probability vectors.

In this continuation, we evaluate the Adversarial Success Rate (ASR) under these modified attack settings, as presented in Tab. S7. This evaluation demonstrates the efficacy of our attack formulation even when faced with the challenge of targeting the least-likely labels.

## S6. More visual examples

For enhanced qualitative evaluation, we offer additional visual examples showcasing successful transformation-dependent adversarial instances against image classification models in Fig. S1 and Fig. S2. Moreover, we present further examples of selective hiding attacks targeting object detection models in Fig. S3, Fig. S4, and Fig. S5.

The examples in Fig. S1 and Fig. S2 illustrate that with imperceptible noise perturbation, an image can be misclassified as multiple target labels when subjected to specific image transformations.

In the case of selective hiding attacks, consider the images in the first row of Fig. S3 as an illustration. It demonstrates that in the clean image, objects labeled as three distinct categories (*person*, *ski*, and *snowboard*) are detected. However, upon adding scale-dependent perturbations, objects labeled as one of these categories become hidden in three differently scaled versions of perturbed images, as depicted in the titles:  $0.5\times$  — *Hide "person"*,  $1.0\times$  — *Hide "ski"*, and  $1.5\times$  — *Hide "snowboard"*.

Table S5. Flip-dependent targeted attack success rate (ASR). ASRs are reported at each target flip version of image and average over all three flipping methods. Higher value indicates better attack performance. The perturbation budget is  $\|\delta\|_\infty \leq 10$ . Below is the model classification accuracy (ACC) evaluation over flipped clean images without perturbation.

Flipping method	Classifier model					
	VGG19	ResNet50	Dense-121	Inc-v3	ViT-L16	ViT-L32
ASR (%) $\uparrow$						
None	100.0	99.90	99.80	92.30	94.10	87.30
Horizontal	100.0	99.90	99.90	91.20	92.90	87.10
Vertical	100.0	99.70	99.90	98.40	96.60	92.50
Average	100.0	99.83	99.87	93.97	94.53	88.97
ACC (%) $\uparrow$						
None	90.80	93.20	94.50	79.90	92.70	89.90
Horizontal	91.70	92.20	94.10	79.60	93.00	90.10
Vertical	54.00	57.50	60.20	40.20	69.60	53.30
Average	78.83	80.97	82.93	66.57	85.10	77.76

Table S6. Perspective-dependent targeted attack success rate (ASR). ASRs are reported at each target flip version of image and average over all three flipping methods. Higher value indicates better attack performance. The perturbation budget is  $\|\delta\|_\infty \leq 10$ . Below is the model classification accuracy (ACC) evaluation over perspective transformed clean images without perturbation.

Perspective	Classifier Model					
	VGG-19	ResNet-50	Dense-161	Inc-v3	ViT-L-16	ViT-L-32
ASR (%) $\uparrow$						
1	100.0	99.90	99.70	93.00	95.90	91.30
2	99.60	98.50	99.30	89.10	84.70	70.70
3	100.0	99.10	99.70	92.20	84.90	72.40
Average	99.87	99.17	99.57	91.43	88.50	78.13
ACC (%) $\uparrow$						
1	90.80	93.20	94.50	79.90	92.70	89.90
2	72.10	72.10	73.50	53.00	87.80	79.30
3	73.60	75.40	74.10	57.90	87.50	78.20
Average	78.83	80.23	80.70	63.60	89.33	82.47



Table S7. ASR evaluation of transformation-dependent attacks using 3 most least-likely labels as targets. Higher value indicates better attack performance. The perturbation budget is  $\|\delta\|_\infty \leq 10$ .

Transform parameter	Classifier model ACC(%) $\uparrow$					
	VGG-19	ResNet-50	Dense-161	Inc-v3	ViT-L-16	ViT-L-32
Scaling						
$S = 0.5$	98.60	89.60	92.10	77.70	81.70	65.40
$S = 1.0$	100.0	99.70	99.70	91.00	95.40	85.80
$S = 1.5$	100.0	99.40	99.00	82.50	91.80	78.00
Average	99.53	96.23	96.93	83.73	89.63	76.40
Blurring						
$\sigma = 0.5$	100.0	99.80	99.90	90.60	94.40	88.70
$\sigma = 1.5$	99.30	96.90	98.20	77.70	74.80	65.60
$\sigma = 3.0$	99.40	95.60	98.20	74.50	71.20	55.90
Average	99.57	97.43	98.77	80.93	80.13	70.07
Gamma						
$\gamma = 0.5$	100.0	99.60	99.80	91.90	98.40	90.90
$\gamma = 1.0$	100.0	99.90	100.0	90.70	94.40	88.00
$\gamma = 2.0$	100.0	99.60	99.70	89.10	85.60	76.80
Average	100.0	99.70	99.83	90.57	93.47	85.23
JPEG						
$Q = 20$	84.20	89.00	65.60	62.20	79.60	73.70
$Q = 50$	95.80	97.00	88.70	74.40	86.00	79.70
$Q = 80$	98.80	98.90	96.00	79.50	88.80	79.40
Average	92.93	94.97	83.43	72.03	84.80	77.60

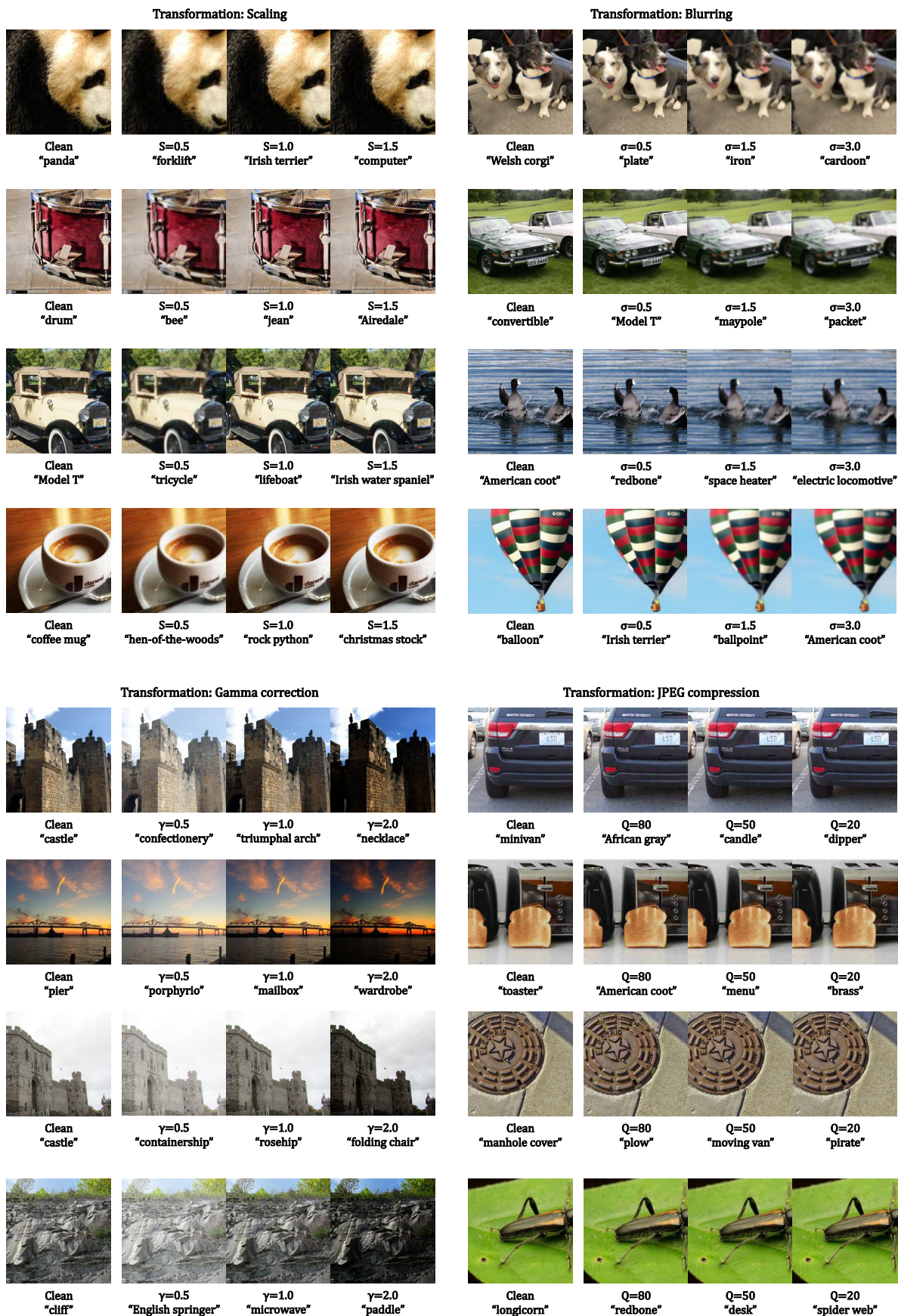


Figure S1. Visualize examples for transform-dependent attacks against image classifiers. In this figure, we show visual effects of clean image and the perturbed images transformed with different parameters.



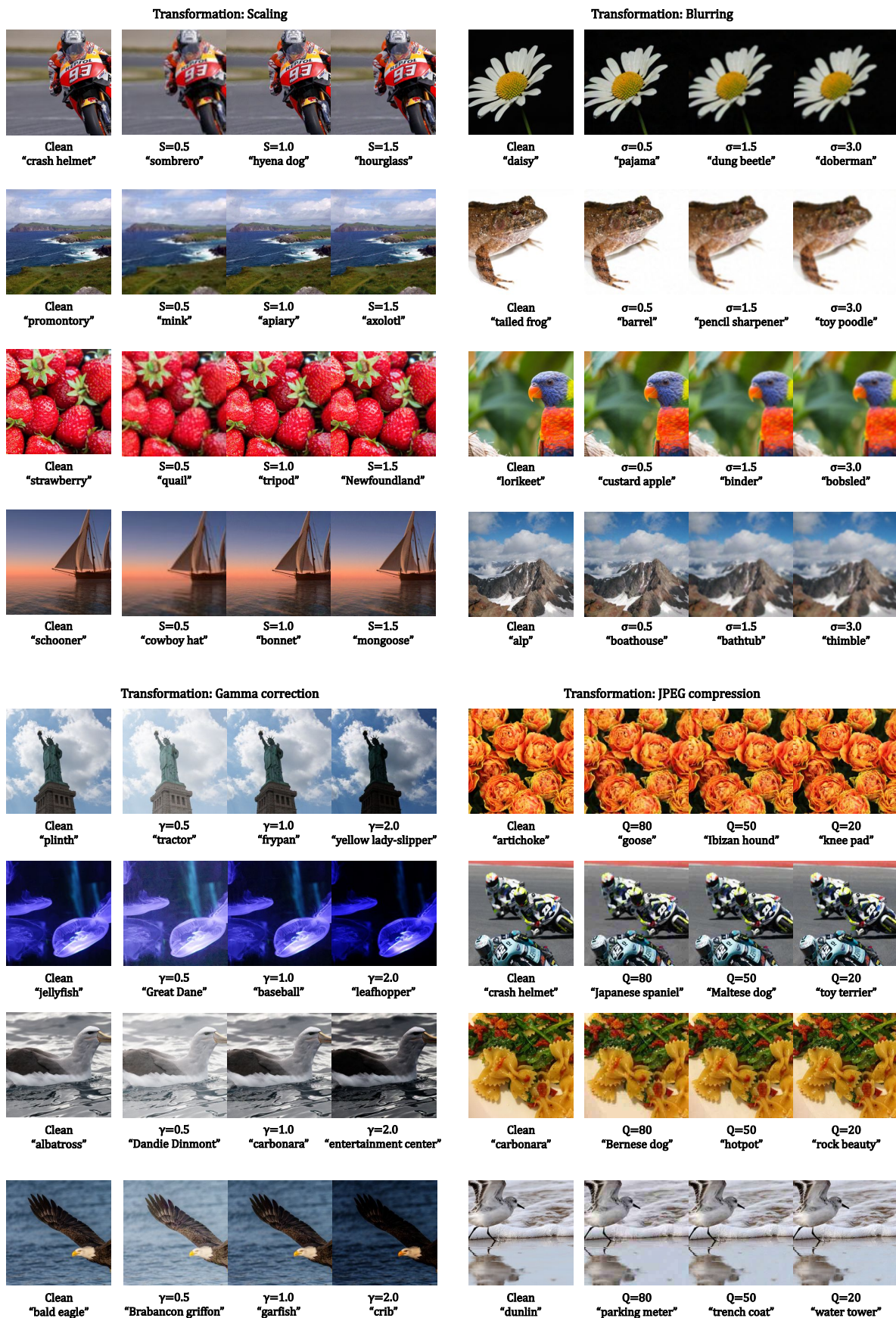


Figure S2. Visualize examples for transform-dependent attacks against image classifiers. In this figure, we show visual effects of successful attacks under different image transformations with different transform parameters.

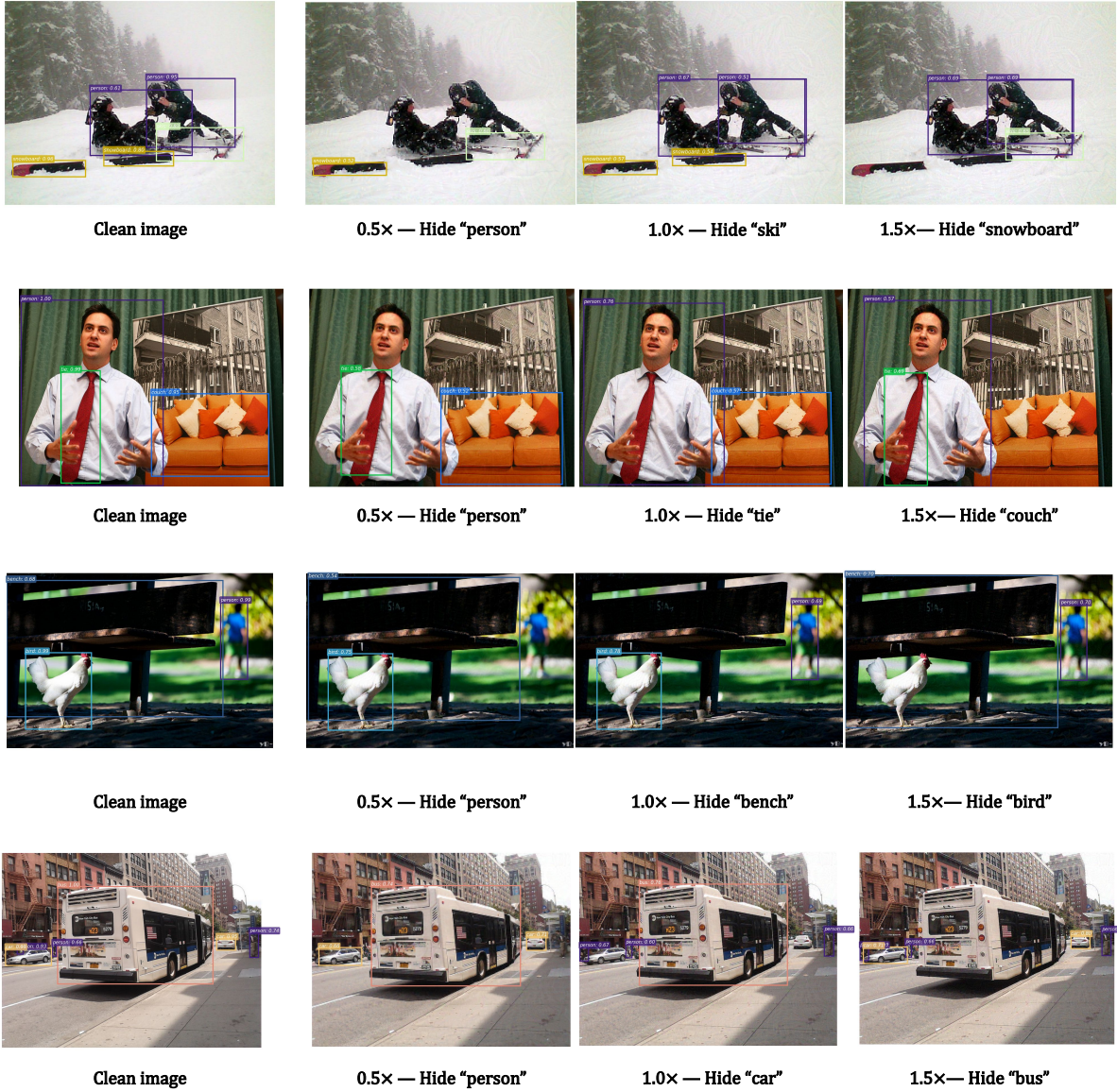
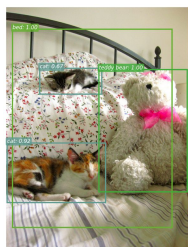
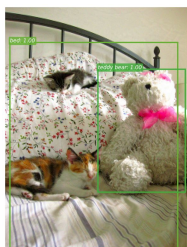


Figure S3. Visualize examples of scale-dependent selective hiding attacks against object detection model FCOS. From top to bottom, ImageIDs: 000000142790, 000000170099, 000000197870, 000000338625. Note, images labeled as 0.5, 1.5x are in resolutions different from the original image, and they are resized to the same size for better display.

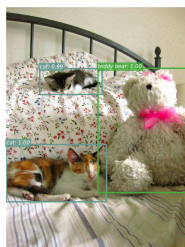




Clean image



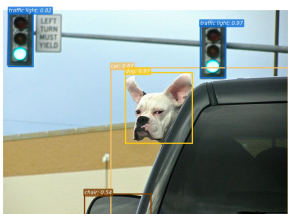
0.5× — Hide “cat”



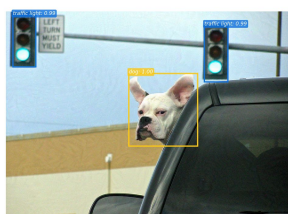
1.0× — Hide “bed”



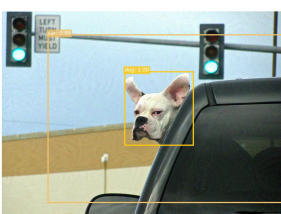
1.5× — Hide “teddy bear”



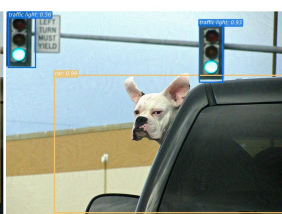
Clean image



0.5× — Hide “car”



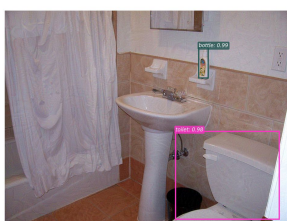
1.0× — Hide “traffic light”



1.5× — Hide “dog”



Clean image



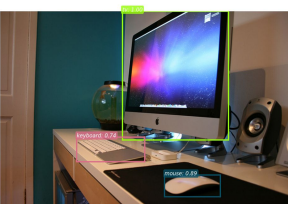
0.5× — Hide “sink”



1.0× — Hide “toilet”



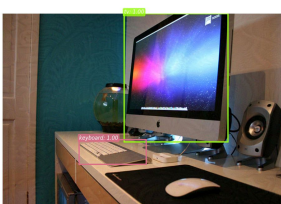
1.5× — Hide “bottle”



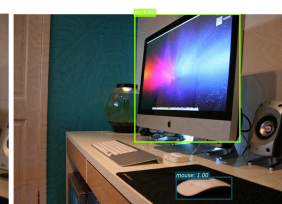
Clean image



0.5× — Hide “TV”



1.0× — Hide “mouse”



1.5× — Hide “keyboard”

Figure S4. Visualize examples of scale-dependent selective hiding attacks against object detection model YOLOv3. From top to bottom, ImageIDs: 000000478393, 000000076417, 000000167898, 000000186282. Note, images labeled as 0.5, 1.5× are in resolutions different from the original image, and they are resized to the same size for better display.

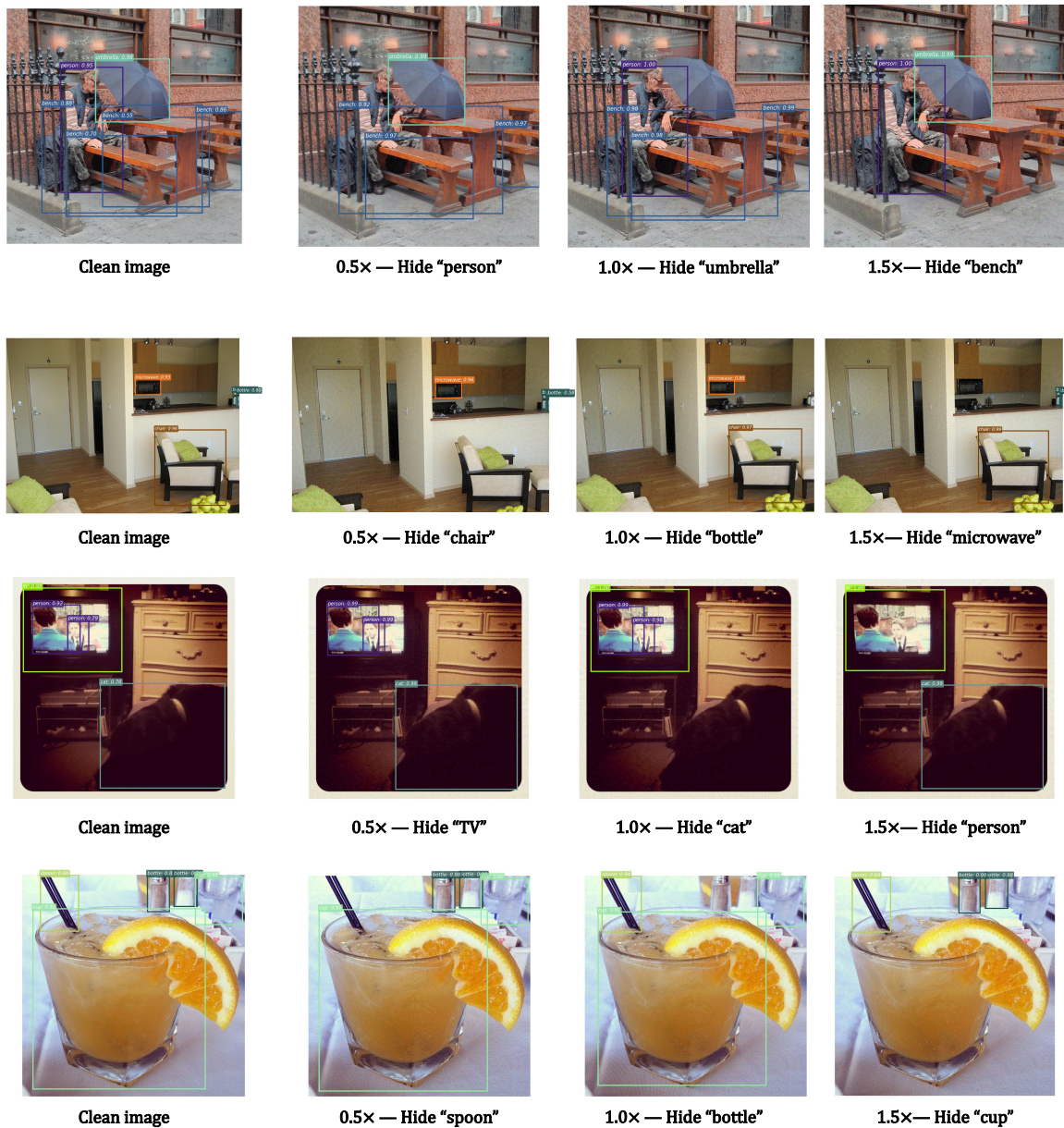


Figure S5. Visualize examples of scale-dependent selective hiding attacks against object detection model Faster R-CNN. From top to bottom, ImageIDs: 000000455157, 000000488075, 000000169076, 000000463283. Note, images labeled as 0.5, 1.5× are in resolutions different from the original image, and they are resized to the same size for better display.